

Tidal Shocking by Extended Mass Distributions

Oleg Y. Gnedin

Princeton University Observatory, Princeton, NJ 08544;
 ognedin@astro.princeton.edu

Lars Hernquist¹

University of California, Santa Cruz, CA 95064;
 lars@ucolick.org

Jeremiah P. Ostriker

Princeton University Observatory, Princeton, NJ 08544;
 jpo@astro.princeton.edu

ABSTRACT

We derive expressions for the tidal field exerted by a spherically symmetric galaxy having an extended mass distribution, and use our analysis to calculate tidal perturbations and heating of stars in a globular cluster or a satellite galaxy orbiting in the external potential. We consider a Hernquist model and several power-law models for the primary. We integrate the tidal force over accurate orbits in the given potential by using the impulse approximation and by introducing adiabatic corrections that allow for the time variation of the force. We compare these results with the conventional straight path approximation. We also check the results with direct N-body simulations and find very good agreement. Heating on highly eccentric orbits dominates as the adiabatic corrections strongly damp the energy change on low eccentricity orbits. The results are illustrated for the example of globular cluster NGC 6712. For the orbital eccentricities higher than 0.9 the future lifetime of NGC 6712 is less than 10^{10} yr. Our analysis can be used to study tidal interactions of star clusters and galaxies in a semi-analytical manner.

Subject headings: globular clusters: general – galaxies: interactions

1. Introduction

Tidal forces are very important in stellar systems. They determine the dynamics of interactions between galaxies in clusters, between a dwarf satellite and a primary galaxy, and between star

¹Presidential Faculty Fellow

clusters and their host galaxies. The most dramatic tidal perturbations occur in fast and close encounters. When the duration of the encounter is shorter than the characteristic dynamical time within the system, such an interaction is referred to as a *tidal shock* (Spitzer 1987).

Previous semi-analytic and numerical studies of tidal shocks considered the primary galaxy as a point-mass (Spitzer 1958; Richstone 1975; Knobloch 1976; Aguilar & White 1985). Such an approximation is violated when the satellite is well within the limits of the galaxy. For example, when globular clusters pass near (or inside) the galactic bulge, we need to take into account the extended mass distribution of the nucleus. In this paper, we obtain expressions for the tidal field of an arbitrary spherically-symmetric system. We then apply them to estimate the amount of heating of stars produced by an interaction.

The paper is organized so that we move from the simplest and least accurate treatment to the more complex and more accurate. We present analytical calculations of the tidal field and velocity changes for a straight-line orbit in §2 and for the eccentric orbits in §3, where we drop the impulse approximation and allow for the protection given by adiabatic invariants for the short period orbits in the satellite system. Some tedious integrals are relegated to the Appendix. Then, in §4, we apply our theory to calculate the heating of globular cluster NGC 6712. In §5 we summarize the relevance of our results to semi-analytic studies of tidal interactions in stellar systems.

2. Tidal perturbation in the straight-path encounter

Consider an inertial reference frame with the origin at the Galactic center. Let $\mathbf{R}_0(t)$ be the trajectory of the center of the satellite, and let r be the distance of a member star from the satellite center. Then the radius-vector of each star from the origin is $\mathbf{R} = \mathbf{R}_0(t) + \mathbf{r}$. The equations of motion for each star are

$$\ddot{\mathbf{R}} = -\frac{\partial\Phi_c}{\partial\mathbf{R}} - \frac{\partial\Phi_G}{\partial\mathbf{R}}, \quad (1)$$

or

$$\ddot{\mathbf{R}}_0 + \ddot{\mathbf{r}} = -\left(\frac{\partial\Phi_G}{\partial\mathbf{R}_0}\right)_{R_0} - \left(\frac{\partial\Phi_c}{\partial\mathbf{r}}\right)_R - \left(\frac{\partial^2\Phi_G}{\partial\mathbf{R}_0\partial\mathbf{R}_0}\right)_{R_0} \cdot \mathbf{r} - \dots \quad (2)$$

where Φ_c and Φ_G are the potentials of the satellite and the galaxy, respectively, and we will drop the subscripts henceforth. The motion of the satellite is determined by the leading terms, $\ddot{\mathbf{R}}_0 = -\partial\Phi_G/\partial\mathbf{R}_0$, so, in the tidal approximation, we have

$$\ddot{\mathbf{r}} = -\frac{\partial\Phi_c}{\partial\mathbf{r}} - \frac{\partial^2\Phi_G}{\partial\mathbf{R}_0\partial\mathbf{R}_0} \cdot \mathbf{r}. \quad (3)$$

The potential of a spherically-symmetric system is

$$\Phi_G = -\frac{GM(R)}{R} - 4\pi G \int_R^\infty \rho(r')r'dr', \quad (4)$$

which produces a tidal force per unit mass

$$\mathbf{F}_{\text{tid}} \equiv - \left(\frac{\partial^2 \Phi_G}{\partial \mathbf{R}_0 \partial \mathbf{R}_0} \right) \cdot \mathbf{r} = \frac{GM_0}{R_0^3} [(3\mu - \dot{\mu})(\mathbf{n} \cdot \mathbf{r})\mathbf{n} - \mu \mathbf{r}], \quad (5)$$

where M_0 is the total mass of the galaxy, and $\mu(R)$ is its normalized mass profile:

$$\mu(R) \equiv \frac{M(R)}{M_0}, \quad (6)$$

and $\dot{\mu}$ is defined by

$$\dot{\mu}(R) \equiv \frac{d\mu(R)}{d \ln R}. \quad (7)$$

The direction to the center of the satellite is denoted by $\mathbf{n} \equiv \mathbf{R}_0/R_0$.

The treatment so far in this section is general. We will now temporarily restrict ourselves to the impulse approximation and straight line orbits for simplicity in the computation. In the impulse approximation we neglect internal motions of the satellite stars during the encounter. The corresponding change in each star's velocity is the integral

$$\Delta \mathbf{v} = \int \mathbf{F}_{\text{tid}} dt \quad (8)$$

over the duration of the interaction. This time-varying perturbation leads to an increase of the random motion (or heating) of stars in the satellite. When the stars are well phase-mixed, the phase space averaged change in their energy is quadratic in the perturbation:

$$\langle \Delta E \rangle = \frac{1}{2} \langle (\Delta v)^2 \rangle. \quad (9)$$

In the impulse approximation we have also neglected the self-consistent reaction of the potential of the satellite as it settles into a new post-shock equilibrium. Effects of the potential readjustment are studied elsewhere (Gnedin & Ostriker 1997b).

To calculate the velocity kick, $\Delta \mathbf{v}$, we need to specify the satellite orbit. Since the tidal force is short-range, only the part of the orbit within a few distances of closest approach (perigalacticon R_p) is important. Therefore the orbit is conventionally assumed to be a straight path, $\mathbf{R}_0(t) = (R_p, V_p t, 0)$, where V_p is the orbital velocity at perigalacticon. For fast encounters, the scattering angle is usually small and the satellite does not deviate much from the original straight path (Knobloch 1976). In §3 we consider eccentric satellite orbits.

Integrating equation (8) from $-\infty$ to ∞ , we find

$$\Delta \mathbf{v} = \frac{2GM_0}{R_p^2 V_p} \{(3J_0 - J_1 - I_0)x, (2I_0 - I_1 - 3J_0 + J_1)y, -I_0 z\}, \quad (10)$$

where

$$I_0(R_p) \equiv \int_1^\infty \mu(R_p \zeta) \frac{d\zeta}{\zeta^2 (\zeta^2 - 1)^{1/2}}, \quad (11a)$$

$$I_1(R_p) \equiv \int_1^\infty \dot{\mu}(R_p \zeta) \frac{d\zeta}{\zeta^2 (\zeta^2 - 1)^{1/2}}, \quad (11b)$$

$$J_0(R_p) \equiv \int_1^\infty \mu(R_p \zeta) \frac{d\zeta}{\zeta^4 (\zeta^2 - 1)^{1/2}}, \quad (11c)$$

$$J_1(R_p) \equiv \int_1^\infty \dot{\mu}(R_p \zeta) \frac{d\zeta}{\zeta^4 (\zeta^2 - 1)^{1/2}}. \quad (11d)$$

Notice also that

$$I_1 = R_p \frac{dI_0}{dR_p}, \quad J_1 = R_p \frac{dJ_0}{dR_p}. \quad (12)$$

Averaging over an ensemble of stars in a spherically-symmetric satellite, we have $\langle x^2 \rangle = \langle y^2 \rangle = \langle z^2 \rangle = r^2/3$. The heating term per unit mass is therefore

$$\langle \Delta E \rangle = \left(\frac{2G M_0}{R_p^2 V_p} \right)^2 \frac{r^2}{3} \chi_{st}(R_p), \quad (13)$$

$$\chi_{st} \equiv \frac{1}{2} \left[(3J_0 - J_1 - I_0)^2 + (2I_0 - I_1 - 3J_0 + J_1)^2 + I_0^2 \right]. \quad (14)$$

These results generalize the usual expressions for a point-mass (e.g. Binney & Tremaine 1987) to the case of an arbitrary spherical density profile. In particular, the function $\chi_{st}(R_p)$ is the correction due to the extended mass distribution of the galaxy. If all the galactic mass were concentrated at its center, then $\mu = 1$ and $\dot{\mu} = 0$ everywhere,

$$I_0 = \int_1^\infty \frac{d\zeta}{\zeta^2 (\zeta^2 - 1)^{1/2}} = 1, \quad J_0 = \int_1^\infty \frac{d\zeta}{\zeta^4 (\zeta^2 - 1)^{1/2}} = \frac{2}{3}, \quad (15)$$

and $I_1 = J_1 = 0$. The factor χ_{st} becomes unity in this case, as expected. The subscript “st” reminds us that this factor is valid for the straight path approximation.

The second order energy diffusion term to lowest order is

$$\langle \Delta E^2 \rangle = \langle (\mathbf{v} \cdot \Delta \mathbf{v})^2 \rangle = \left(\frac{2G M_0}{R_p^2 V_p} \right)^2 \frac{2r^2 v^2 (1 + \chi_{r,v})}{9}, \quad (16)$$

where $\chi_{r,v}$ is the position-velocity correlation function (see Gnedin & Ostriker 1997b). This can be simply rewritten as

$$\langle \Delta E^2 \rangle = \frac{2v^2 (1 + \chi_{r,v})}{3} \langle \Delta E \rangle. \quad (17)$$

Aguilar & White (1985) conducted numerical N-body experiments for encounters of spherical systems and proposed a correction term of the form $\chi_{AW} = 1/2 I_0^2$ (in our notation). This factor is everywhere smaller than the full function χ_{st} (eq. [14]). We have compared these correction factors for the spheroidal components of two models of our Galaxy available in the literature: the Ostriker & Caldwell (1983) model and the Bahcall, Schmidt, & Soneira (1983) model. Figure 1 shows that the difference between χ_{st} and χ_{AW} is small inside 1 kpc, but rises steadily with increasing perigalactic distance. In the limit of large R_p , our function χ_{st} approaches unity whereas χ_{AW} remains short of it by about a factor of 2.

2.1. The Hernquist model

For illustration, we consider here two example mass distributions, the Hernquist model (Hernquist 1990) and power-law density profiles. The Hernquist model closely resembles the $R^{1/4}$ law for spherical galaxies and gives simple analytical expressions for the potential-density pair:

$$\Phi = -\frac{GM_0}{R+a}, \quad \rho = \frac{M_0 a}{2\pi R(R+a)^3}, \quad (18)$$

where M_0 is the total mass of the model, and a is the scale length of the potential. The normalized mass profile is

$$\mu(R) = \frac{R^2}{(R+a)^2}, \quad \dot{\mu}(R) = \frac{2aR^2}{(R+a)^3}. \quad (19)$$

Calculation of the integrals (11) is given in Appendix A. The results (eq. [A9]) are plotted in Figure 2 as function of $\alpha \equiv a/R_p$.

For large impact parameters ($\alpha \ll 1$), I_0 and J_0 approach constant values ($I_0 = 1$, $J_0 = 2/3$) and I_1 and J_1 decrease linearly with α . As a result, the satellite is compressed in the vertical direction, stretched in the direction of the perigalacticon by the same amount, and there is no net effect in the perpendicular direction. All this is expected in the point-mass approximation. At very small impact parameters ($\alpha \gg 1$) when the satellite penetrates within a scale length of the center, all the correction factors decline approximately as α^{-2} . This asymptotic behavior is due to the mass of the model increasing quadratically with radius at small r .

In Figure 3 we plot the absolute value of the components of the velocity change for the Hernquist model:

$$\chi_x \equiv 3J_0 - J_1 - I_0 \quad (20a)$$

$$\chi_y \equiv 2I_0 - I_1 - 3J_0 + J_1 \quad (20b)$$

$$\chi_z \equiv I_0 \quad (20c)$$

Note that χ_x and χ_z are the velocity changes in the x and z directions relative to their values in the point-mass approximation. The velocity change in the y direction (Δv_y) is almost negligible for any α , with $\chi_y \sim 10^{-4}$. In the point-mass approximation, $\Delta v_y \equiv 0$. Also, we plot for comparison the naive correction assuming the galactic mass inside the perigalacticon R_p to be a point-mass. The correction factor in this case is $\chi_{x0} = \chi_{z0} = \chi_0 \equiv \mu(R_p)$. It underestimates the vertical compression, but overestimates the effect in the radial direction.

2.2. The power-law model

Next, we consider a general power-law distribution truncated at a limiting radius R_{max} ,

$$\rho(R) = \begin{cases} k R^{-n}, & R \leq R_{max} \quad (n < 3) \\ 0, & R > R_{max} \end{cases} \quad (21)$$

Here k is a constant that determines the total mass of the model, $M_0 = \frac{4\pi k}{3-n} R_{max}^{3-n}$. We assume that the perturbed satellite is well within the extent of the galaxy so that truncation of the model will not affect our results. The normalized mass profile is

$$\mu(R) = \left(\frac{R}{R_{max}} \right)^{3-n}, \quad \dot{\mu}(R) = (3-n) \mu(R). \quad (22)$$

Evaluation of the tidal integrals is straightforward:

$$I_0 = \left(\frac{R_p}{R_{max}} \right)^{3-n} \int_1^\infty \frac{\zeta^{1-n} d\zeta}{(\zeta^2 - 1)^{1/2}} = \left(\frac{R_p}{R_{max}} \right)^{3-n} \frac{\sqrt{\pi}}{2} \frac{\Gamma\left(\frac{n-1}{2}\right)}{\Gamma\left(\frac{n}{2}\right)}, \quad I_1 = (3-n) I_0. \quad (23a)$$

$$J_0 = \left(\frac{R_p}{R_{max}} \right)^{3-n} \int_1^\infty \frac{\zeta^{-1-n} d\zeta}{(\zeta^2 - 1)^{1/2}} = \left(\frac{R_p}{R_{max}} \right)^{3-n} \frac{\sqrt{\pi}}{2} \frac{\Gamma\left(\frac{n+1}{2}\right)}{\Gamma\left(\frac{n+2}{2}\right)}, \quad J_1 = (3-n) J_0. \quad (23b)$$

Note that the integral for I_0 converges only for $n > 1$. Using the identity $\Gamma(x+1) = x\Gamma(x)$, we find $n J_0 = (n-1) I_0$.

The change in the velocity of a star is

$$\Delta \mathbf{v} = \frac{GM_0}{R_p^2 V_p} \left(\frac{R_p}{R_{max}} \right)^{3-n} \frac{\sqrt{\pi} \Gamma\left(\frac{n-1}{2}\right)}{\Gamma\left(\frac{n}{2}\right)} \{(n-2)x, 0, -z\}, \quad (24)$$

where the y -component vanishes because of the symmetry of the trajectory. The correction to the energy change is

$$\chi_{st} = \left(\frac{R_p}{R_{max}} \right)^{6-2n} \left[\frac{\Gamma\left(\frac{n-1}{2}\right)}{\Gamma\left(\frac{n}{2}\right)} \right]^2 \frac{\pi(n^2 - 4n + 5)}{8}. \quad (25)$$

We remind the reader that this result holds for the power-law indices $1 < n < 3$.

Note the change in sign of the x -component of $\Delta \mathbf{v}$ as n passes through the value $n = 2$. For the special case of an isothermal sphere ($n = 2$), the x -component of the velocity change vanishes identically and the only resulting change is compression in the vertical direction:

$$\Delta \mathbf{v} = -\frac{GM_0}{R_p^2 V_p} \frac{\pi R_p}{R_{max}} \mathbf{z}, \quad \chi_{st}(R_p) = \frac{\pi^2}{8} \frac{R_p^2}{R_{max}^2}. \quad (26)$$

3. Tidal perturbation on eccentric orbits

The straight-path orbit is a convenient approximation, but in real galaxies, satellites move on eccentric orbits with the tidal shocks strongly concentrated to the epoch of perigalacticon. And in the opposite limit, the circular orbit, there is no effect at all. The results obtained in the previous section should nevertheless give us insight into the actual heating of satellites on eccentric orbits.

In this section, we determine the true orbits in our examples of galactic models and investigate how tidal heating depends on parameters of the orbit.

In a spherically-symmetric potential the orbit of a satellite is confined to a plane and can be characterized by two independent parameters. Let us choose the perigalactic distance, R_p , and eccentricity, e , as such parameters. They in turn determine the energy and angular momentum of the orbit. We employ polar coordinates in which the position angle $\theta(t)$ can be used as a time variable. This angle is defined such that $\theta = 0$ at $R = R_p$. In the coordinate frame where the orbit is in the XY plane, the position vector of the satellite is $\mathbf{n}(t) = \hat{\mathbf{x}} \cos \theta(t) + \hat{\mathbf{y}} \sin \theta(t)$.

Using the impulse approximation, we integrate the tidal force along the orbit to obtain the expected change in the stellar velocity in the satellite:

$$\Delta \mathbf{v} = \int_{-T/2}^{T/2} \mathbf{F}_{\text{tid}} dt, \quad (27)$$

where T is the orbital period.

Changing the variable of integration from time, t , to the angle, θ , using the identity $dt = (R^2/J) d\theta$, where J is the orbital angular momentum, we obtain

$$\Delta \mathbf{v} = \left(\frac{GM_0}{a^3} \right)^{1/2} \int_{-\theta_m}^{\theta_m} d\theta \frac{a}{jR} [(3\mu - \mu) (\mathbf{n} \cdot \mathbf{r}) \mathbf{n} - \mu \mathbf{r}], \quad (28)$$

where a is the parameter of the galactic model (R_{\max} in case of the power-law models), and j is the dimensionless angular momentum, defined by $J \equiv (GM_0 a)^{1/2} j$. Note that the integration over the position angle extends to the maximum angle θ_m corresponding to the apogalactic point of the orbit. Therefore, the tidal force is integrated starting from the apogalacticon at $\theta = -\theta_m$, approaching the perigalacticon at $\theta = 0$, and going to the next apogalacticon at $\theta = \theta_m$. The maximum position angle ranges from $\theta_m = \pi$ in the Keplerian potential to $\theta_m = \pi/2$ in the harmonic oscillator potential. A very accurate procedure for calculating the orbits is described in Appendix B.

Rewriting the velocity change into components, we have

$$\Delta \mathbf{v} = \left(\frac{GM_0}{a^3} \right)^{1/2} \frac{1}{j(\alpha, e)} \{(B_1 - B_3)x, (B_2 - B_3)y, -B_3z\}, \quad (29)$$

where

$$B_1 = \int_{-\theta_m}^{\theta_m} \frac{3\mu(R) - \mu(R)}{R/a} \cos^2 \theta d\theta \quad (30a)$$

$$B_2 = \int_{-\theta_m}^{\theta_m} \frac{3\mu(R) - \mu(R)}{R/a} \sin^2 \theta d\theta \quad (30b)$$

$$B_3 = \int_{-\theta_m}^{\theta_m} \frac{\mu(R)}{R/a} d\theta. \quad (30c)$$

Because of the symmetry of the orbit, $R(\theta) = -R(\theta)$, the cross-terms ($\propto xy$) vanish.

The changes in the energy of the star are

$$\langle \Delta E \rangle = \frac{GM_0}{a^3} r^2 \frac{(B_1 - B_3)^2 + (B_2 - B_3)^2 + B_3^2}{6j^2(\alpha, e)} A_1(x_t). \quad (31)$$

$$\langle \Delta E^2 \rangle = \frac{GM_0}{a^3} \frac{2r^2 v^2 (1 + \chi_{r,v})}{3} \frac{(B_1 - B_3)^2 + (B_2 - B_3)^2 + B_3^2}{6j^2(\alpha, e)} A_2(x_t). \quad (32)$$

We have added here the adiabatic corrections $A_1(x_t)$ and $A_2(x_t)$ that allow for the reduction of the energy input due to conservation of adiabatic invariants of stars which occur when the orbital period of stars in the satellite is shorter than the time duration of the external force. Gneden & Ostriker 1997b provide a detailed discussion of the adiabatic corrections in the case of disk shocking. The main result can be summarized as follows. The actual change of the stellar energy, as inferred from the N-body modeling of the shock, is described to good accuracy by the product of the energy change in the impulse approximation and the adiabatic correction of the form

$$A_1(x_t) = (1 + x_t^2)^{-\gamma}, \quad (33)$$

where $\gamma \approx 1.5$, and $x_t \equiv \omega(r)\tau$. Here $\omega(r)$ is the orbital frequency of the stellar motion in the satellite, and τ is the effective timescale of the shock. The adiabatic correction becomes increasingly small in the core of the satellite, preserving stellar energy and adiabatic integrals. At the tidal radius of the satellite, A_1 approaches unity. While the index γ may depend on the cluster concentration and other parameters (see also Weinberg 1994), we believe that equation (33) provides sufficient accuracy for our purpose. Numerical tests with the more concentrated cluster ($c = 1.5$) also support our formalism.

The adiabatic correction depends not only on the position r of the star in the satellite, but also on the eccentricity of the cluster orbit through the parameter τ . As Aguilar, Hut, & Ostriker (1988) pointed out, there should be no heating in a satellite on a circular orbit because in this case the external potential is constant in time and the energy is conserved. Since on the circular orbit the effective duration of the shock, τ , becomes infinitely long, the adiabatic correction becomes zero and the stellar energy is indeed conserved. We will return to the adiabatic corrections in §4, when we consider an example of a globular cluster NGC 6712.

3.1. The Hernquist model

It is of interest to compare the results for the satellites on eccentric orbits with those on the straight path. For the Hernquist model we perform the integration of equations (30) numerically for a grid of perigalactica and eccentricities. We now rewrite equation (31) for $\langle \Delta E \rangle$ similarly to equation (13), extracting the factor $\chi_{ecc}(\alpha, e)$ which now is a function of $\alpha \equiv a/R_p$ and e . For clarity, the factor $\chi_{ecc}(\alpha, e)$ does not include the adiabatic correction $A_1(x_t)$.

Figure 4 shows the ratio χ_{ecc}/χ_{st} for the orbits with various eccentricities. For highly eccentric orbits, $e \lesssim 1$, the ratio varies slightly with α , from $\chi_{ecc}/\chi_{st} \approx 1.8$ for $\alpha \ll 1$ to $\chi_{ecc}/\chi_{st} = 1$ for $\alpha \gg 1$. The latter limit corresponds to the most eccentric Keplerian orbit where both approaches must agree.

However, as the eccentricity decreases, the ratio χ_{ecc}/χ_{st} falls faster with α . While the ratio is the highest for $e = 0$ at $\alpha \ll 1$, the opposite is true for $\alpha \gg 1$.

3.2. The power-law models

The power-law models are scale-free and allow us to further simplify equations (30). Taking out all the powers of $\alpha \equiv R_{max}/R_p$, we have

$$\langle \Delta E \rangle = \frac{G M_0}{R_{max}^3} r^2 \alpha^n \chi_{ecc}(e) A_1(x_t), \quad (34)$$

$$\chi_{ecc} \equiv \frac{(C_1 - C_3)^2 + (C_2 - C_3)^2 + C_3^2}{6f(e)}, \quad (35)$$

where $B_i(\alpha, e) \equiv \alpha^{n-2} C_i(e)$, and $j^2(\alpha, e) \equiv \alpha^{n-4} f(e)$. The remaining integrals depend only on the eccentricity e . After some algebra, we obtain

$$C_1 = n \int_{-\theta_m}^{\theta_m} \left(\frac{R}{R_p} \right)^{2-n} \cos^2 \theta d\theta, \quad (36a)$$

$$C_2 = n \int_{-\theta_m}^{\theta_m} \left(\frac{R}{R_p} \right)^{2-n} \sin^2 \theta d\theta, \quad (36b)$$

$$C_3 = \int_{-\theta_m}^{\theta_m} \left(\frac{R}{R_p} \right)^{2-n} d\theta. \quad (36c)$$

Note that in the harmonic oscillator potential ($n = 0$), the first two integrals are identically zero: $C_1 = C_2 = 0$. The third one can be done using the simple analytic orbits in this potential (eq. [B4]).

$$C_3 = \pi \frac{1+e}{1-e}, \quad \chi_{ecc} = \frac{\pi^2}{2} \quad (\text{for } n = 0). \quad (37)$$

Surprisingly enough, the change of the stellar energy does not depend on either location in the galaxy, α , or the orbital eccentricity, e .

$$\Delta \mathbf{v} = \left(\frac{G M_0}{R_{max}^3} \right)^{1/2} \pi \{-x, -y, -z\}, \quad (38)$$

$$\langle \Delta E \rangle = \frac{G M_0}{R_{max}^3} \frac{\pi^2}{2} r^2 A_1(x_t) \quad (\text{for } n = 0). \quad (39)$$

The satellite is equally compressed in all directions.

In the isothermal sphere potential ($n = 2$), the integrals are also done straightforwardly:

$$C_1 = 2\theta_m + \sin 2\theta_m, \quad (40a)$$

$$C_2 = 2\theta_m - \sin 2\theta_m, \quad (40b)$$

$$C_3 = 2\theta_m, \quad (\text{for } n = 2). \quad (40c)$$

For the $n = 1$ model, the integrals $C_i(e)$ are done numerically. Figure 5 shows the factors χ_{ecc} for all three models. For comparison, we plot χ_{st} for the isothermal sphere. Heating on the eccentric orbits is larger than that on the straight orbit, and the two are asymptotically equal at $e = 1$.

Note that the expression for the energy change (eq. [34]) contains the adiabatic correction $A_1(x_t)$, which effectively reduces the heating on low-eccentricity orbits.

4. A Case Study: NGC 6712

We now illustrate the theory developed in §3 by considering an example of a globular cluster, NGC 6712. This cluster orbits our Galaxy and is presently at 3.8 kpc from the Galactic center, so that it is close enough to experience tidal shocking by the Galactic bulge. We use the observed parameters of the cluster to construct its orbit in the bulge potential and to integrate the expected energy change. Then we perform N-body simulations to verify the result. Finally, we consider various orbital eccentricities the cluster could have with its orbital energy and illustrate the effect of the eccentricity on the resulting heating of the cluster.

4.1. Constructing the orbit

Full three-dimensional kinematic data for NGC 6712 are not yet available. Instead, we use the Monte-Carlo simulations by Gnedin & Ostriker (1997a) for the Ostriker-Caldwell model of the Galaxy with the isotropic velocity distribution of the globular cluster system. The authors draw the two unknown components of the cluster velocity consistent with the chosen kinematic model and integrate the orbits for 10^{10} yr. For NGC 6712, the median perigalactic distance is $R_p = 0.73$ kpc and the velocity at the perigalacticon is $V_p = 396$ km s $^{-1}$. The eccentricity of this orbit is $e = 0.69$.

We approximate the bulge by the Hernquist model with the scale-length $a = 0.6$ kpc. The total mass of the model required to reproduce the observed velocity V_p is $M_0 = 3.3 \times 10^{10} M_\odot$, close to the observed mass of the bulge.

Figure 6 shows the vertical component of the tidal force exerted on the cluster along a single orbit in the Galaxy. The force peaks at the perigalacticon. The dashed line shows that the Gaussian fit to the actual force, $F_{fit} \propto e^{-t^2/\tau^2}$, is accurate for the most important part of the orbit. (A similar parameterization was employed by Johnston, Hernquist & Weinberg 1997 in their numerical study of tidal heating.) The width of the Gaussian, or the effective time-scale of the shock, is $\tau \approx 5.3 t_{dyn}$, where t_{dyn} is the half-mass dynamical time of the cluster, so that most of the stellar orbits in the cluster are strongly protected by adiabatic invariants even for $R_p < 1$ kpc. Using our approximation of the tidal force we estimate the adiabatic corrections to the energy change (cf. eq. [33]) and check them with N-body simulations described next.

4.2. Self-Consistent N-body simulations

We can now simulate the cluster as a system of N point-mass particles and run it along the given orbit. At the end, we calculate the change of the stellar energies and compare them with our analytic theory.

We use a Self-Consistent Field (SCF) code (Hernquist & Ostriker 1992, Gnedin & Ostriker 1997b) with $N = 10^6$ particles. The code approximates the true gravitational potential and density of the cluster with a finite series of basis functions. In this work we take $n = 10$ radial functions and $l = 6$ spherical harmonics.

The initial cluster realization is the King model with the concentration parameter $c = 0.84$. It is sufficiently close to the observed concentration of NGC 6712 of $c \approx 0.9$. The code employs units in which $G = 1$, $M_{cl} = 1$, and $R_c = 1$, where M_{cl} and R_c are the mass and the initial core radius of the cluster. The physical units are fixed by using the observed values of $M_{cl} = 2.5 \times 10^5 M_\odot$ and $R_c = 1.86$ pc.

In this run the gravitational potential of the cluster is kept fixed. The self-consistent response of the system to the tidal perturbation is studied elsewhere (Gnedin & Ostriker 1997b) and is not important for our discussion. We run the cluster along the orbit, starting from the apogalacticon, where the tidal force is minimal (cf. Figure 6), going to the perigalacticon, and then leaving to the next apogalacticon. The whole simulation lasts for about 200 dynamical times, t_{dyn} , of the cluster, with a short enough time step to ensure accurate integration of stellar orbits; $\Delta t = 0.01 t_{dyn}$. We ran the code on the SGI Origin 2000 supercomputer at the Princeton University Observatory.

Figure 7 shows the first and second order energy changes at the end of the simulation. The particles were grouped in equal size bins, ranked by their initial energy, and the means $\langle \Delta E \rangle$, $\langle \Delta E^2 \rangle$ and their standard errors are calculated for each bin. Our analytical estimate (eq. [31]) agrees very well with the numerical result. We applied here the adiabatic corrections in the form of equation (33), with the shock parameter $\tau = 5.3 t_{dyn}$ (see §4.1) and the index $\gamma = 1.4$ for $\langle \Delta E \rangle$ and $\gamma = 1.5$ for $\langle \Delta E^2 \rangle$. We note here that had we used the simplest theory presented in §2 for straight line orbits without adiabatic corrections, we would have overestimated the total energy

change significantly.

The excellent agreement of the theory with the simulations encourages one to use the analytical equations (31), along with the adiabatic corrections in a very simple form, to study the effects of tidal shocks on evolution of globular clusters and satellite galaxies orbiting larger hosts.

4.3. Effects of orbital eccentricity

Finally, we demonstrate how varying eccentricity of the orbit changes the resulting heating. We keep the same orbital energy of NGC 6712 but consider any eccentricity the cluster might have. Since these two parameters (E_{orb} and e) specify the orbit, the perigalactic distance R_p and the parameter α change accordingly with e . Increasing eccentricity decreases R_p as E_{orb} is fixed. Also, low eccentricity orbits have longer shock parameter τ that leads to significant adiabatic corrections.

Figure 8 shows the energy change at the half-mass radius of the cluster, calculated from equation (31). $\langle \Delta E \rangle_h$ falls dramatically with decreasing eccentricity, in part because R_p increases as e decreases and largely because of the adiabatic corrections. As expected, there is no heating on circular orbits.

For comparison, we calculate $\langle \Delta E \rangle_h$ for the two more cases, when the orbital energy is a half and twice the observed value. The more bound orbits tend to have shorter τ and therefore larger energy input than the less bound orbits.

5. Summary

We have calculated the tidal force of a spherical mass distribution. Using the impulse approximation and adiabatic corrections, we estimated the amount of heating of stars in the satellite during a tidal shock by a galaxy. We considered several mass distributions for the galaxy: a Hernquist model and three power-law density profiles, and explored various satellite orbits. We restricted ourselves to spherically-symmetric galaxies to simplify the analysis. Although the actual distribution of the Galactic bulge is probably triaxial, our results should hold for non-spherical systems with modest flattenings.

For the Hernquist model, we found that heating is enhanced by a factor of few on eccentric orbits compared to the conventional straight path approximation. However, adiabatic corrections prevent any heating on low-eccentricity orbits. In the harmonic oscillator potential, the satellite is equally compressed in all directions. In the isothermal sphere potential, heating on eccentric orbits is also larger than that calculated in the straight path approximation.

The results of our calculations are very useful for semi-analytical studies of tidal interactions between large galaxies and their dwarf companions or globular star clusters. For example, Gnedin

& Ostriker (1997a) estimated the amount of heating of globular clusters due to the Galactic bulge by inserting equations (11, 13, 14) into their Fokker-Planck code. Assuming spherical symmetry of the cluster, the code solves the Fokker-Planck equation for the distribution function of stars in energy space. This approach is much faster than a full N-body simulation and allows a direct comparison with analytical models of the clusters.

To illustrate the analytic results (eqs. [31-33]), we considered the example of globular cluster NGC 6712. For a fixed orbital energy of the cluster, the heating is much larger on highly eccentric orbits than on low-eccentricity orbits because of the adiabatic corrections. N-body simulations confirm the validity of our results and demonstrate their power in calculating the tidal heating of satellites orbiting their host galaxies. This semi-analytic method can also be used for studying the evolution of giant star clusters in galactic nuclei or the disruption of dwarf satellites in groups of galaxies.

This work was supported in part by the NSF under grants AST 94-24416 and ASC 93-18185 and the Presidential Faculty Fellows Program.

A. Calculation of the tidal integrals for the Hernquist model

We evaluate here the tidal integrals (eq. [11]) for the Hernquist model. The normalized mass profile is given by equation (19). Denoting $\alpha \equiv a/R_p$, the first integral is

$$I_0(\alpha) = \int_1^\infty \frac{\zeta^2}{(\zeta + \alpha)^2} \frac{d\zeta}{\zeta^2(\zeta^2 - 1)^{1/2}}. \quad (\text{A1})$$

Substituting $x = (\zeta + \alpha)^{-1}$, we have

$$I_0(\alpha) = \int_0^{(1+\alpha)^{-1}} \frac{xdx}{[1 - 2\alpha x + (\alpha^2 - 1)x^2]^{1/2}}. \quad (\text{A2})$$

Now for $\alpha > 1$ we take $y = \alpha - (\alpha^2 - 1)x$, and

$$I_0(\alpha) = (\alpha^2 - 1)^{-3/2} \int_1^\alpha \frac{(\alpha - y)dy}{(y^2 - 1)^{1/2}} = -\frac{1}{\alpha^2 - 1} + \frac{\alpha}{(\alpha^2 - 1)^{3/2}} \ln(\alpha + (\alpha^2 - 1)^{1/2}). \quad (\text{A3})$$

For $\alpha < 1$,

$$I_0(\alpha) = (1 - \alpha^2)^{-3/2} \int_\alpha^1 \frac{(y - \alpha)dy}{(1 - y^2)^{1/2}} = \frac{1}{1 - \alpha^2} - \frac{\alpha}{(1 - \alpha^2)^{3/2}} \arccos \alpha. \quad (\text{A4})$$

It is straightforward to verify that both expressions match smoothly at $\alpha = 1$; $I_0(1) = 1/3$. The next integral, $J_0(\alpha)$, can be reduced to the already calculated I_0 . Taking $x = \zeta^{-1}$,

$$J_0(\alpha) = \int_0^1 \frac{x^3 dx}{(1 + \alpha x)^2(1 - x^2)^{1/2}} = \frac{1}{\alpha^2} \int_0^1 \frac{(\alpha^2 x^2 + 2\alpha x + 1 - 1 - 2\alpha x) x dx}{(1 + \alpha x)^2(1 - x^2)^{1/2}}$$

$$\begin{aligned}
&= \frac{1 - I_0}{\alpha^2} - \frac{2}{\alpha} \int_0^1 \frac{x^2 dx}{(1 + \alpha x)^2 (1 - x^2)^{1/2}} \\
&= \frac{1 + 3I_0}{\alpha^2} - \frac{\pi}{\alpha^3} - \frac{2I_0}{\alpha^4} + \frac{2}{\alpha^4} \int_0^1 \frac{(\alpha + x) dx}{(1 + \alpha x)^2 (1 - x^2)^{1/2}}.
\end{aligned} \tag{A5}$$

Now it is useful to note that

$$\int_0^1 \frac{(\alpha + x) dx}{(1 + \alpha x)^2 (1 - x^2)^{1/2}} \equiv 1 \tag{A6}$$

for all α . Thus we arrive at

$$J_0(\alpha) = \frac{\alpha^2 - \pi\alpha + 2 + (3\alpha^2 - 2)I_0(\alpha)}{\alpha^4}. \tag{A7}$$

The remaining two integrals are easily calculated using the identity (12), or

$$I_1(\alpha) = -\alpha \frac{dI_0(\alpha)}{d\alpha}, \quad J_1(\alpha) = -\alpha \frac{dJ_0(\alpha)}{d\alpha}. \tag{A8}$$

For convenience, all four integrals are combined below.

$$I_0 = \begin{cases} \frac{1}{1-\alpha^2} - \frac{\alpha}{(1-\alpha^2)^{3/2}} \arccos \alpha, & [\alpha < 1] \\ \frac{1}{3} \approx 0.33333, & [\alpha = 1] \\ \frac{1}{1-\alpha^2} + \frac{\alpha}{(\alpha^2-1)^{3/2}} \ln(\alpha + (\alpha^2 - 1)^{1/2}), & [\alpha > 1] \end{cases} \tag{A9a}$$

$$I_1 = \begin{cases} -\frac{3\alpha^2}{(1-\alpha^2)^2} + \frac{\alpha(1+2\alpha^2)}{(1-\alpha^2)^{5/2}} \arccos \alpha, & [\alpha < 1] \\ \frac{4}{15} \approx 0.26667, & [\alpha = 1] \\ -\frac{3\alpha^2}{(\alpha^2-1)^2} + \frac{\alpha(1+2\alpha^2)}{(\alpha^2-1)^{5/2}} \ln(\alpha + (\alpha^2 - 1)^{1/2}), & [\alpha > 1] \end{cases} \tag{A9b}$$

$$J_0 = \begin{cases} \frac{-\alpha^3 + \pi\alpha^2 + 2\alpha - \pi}{\alpha^3(1-\alpha^2)} - \frac{3\alpha^2 - 2}{\alpha^3(1-\alpha^2)^{3/2}} \arccos \alpha, & [\alpha < 1] \\ \frac{10}{3} - \pi \approx 0.19174, & [\alpha = 1] \\ \frac{-\alpha^3 + \pi\alpha^2 + 2\alpha - \pi}{\alpha^3(1-\alpha^2)} + \frac{3\alpha^2 - 2}{\alpha^3(\alpha^2-1)^{3/2}} \ln(\alpha + (\alpha^2 - 1)^{1/2}), & [\alpha > 1] \end{cases} \tag{A9c}$$

$$J_1 = \begin{cases} \frac{2\alpha^5 - 3\pi\alpha^4 - 11\alpha^3 + 6\pi\alpha^2 + 6\alpha - 3\pi}{\alpha^3(1-\alpha^2)^2} + \frac{12\alpha^4 - 15\alpha^2 + 6}{\alpha^3(1-\alpha^2)^{5/2}} \arccos \alpha, & [\alpha < 1] \\ 9.6 - 3\pi \approx 0.17522, & [\alpha = 1] \\ \frac{2\alpha^5 - 3\pi\alpha^4 - 11\alpha^3 + 6\pi\alpha^2 + 6\alpha - 3\pi}{\alpha^3(\alpha^2-1)^2} + \frac{12\alpha^4 - 15\alpha^2 + 6}{\alpha^3(\alpha^2-1)^{5/2}} \ln(\alpha + (\alpha^2 - 1)^{1/2}), & [\alpha > 1] \end{cases} \tag{A9d}$$

B. Orbit integration

We describe here an accurate procedure to calculate orbits in a given potential. The four potentials used in this paper are (in dimensionless units):

$$\phi(r) = -\frac{1}{1+r} \quad (\text{Hernquist model}) \quad (\text{B1a})$$

$$\phi(r) = \frac{r^2}{2} - \frac{3}{2} \quad (\text{harmonic oscillator}) \quad (\text{B1b})$$

$$\phi(r) = r - 2 \quad (n = 1 \text{ power-law model}) \quad (\text{B1c})$$

$$\phi(r) = \ln r - 1 \quad (\text{singular isothermal sphere}). \quad (\text{B1d})$$

First, we specify the angular momentum of the orbit for given α and e . By equating the orbital energy at the perigalacticon and the apogalacticon, we find

$$j^2(\alpha, e) = \frac{(1+e)^2}{\alpha(1+\alpha)(1+\alpha+(1-\alpha)e)} \quad (\text{Hernquist model}) \quad (\text{B2a})$$

$$j^2(\alpha, e) = \alpha^{-4} \frac{(1+e)^2}{(1-e)^2} \quad (\text{harmonic oscillator}) \quad (\text{B2b})$$

$$j^2(\alpha, e) = \alpha^{-3} \frac{(1+e)^2}{1-e} \quad (n = 1 \text{ power-law model}) \quad (\text{B2c})$$

$$j^2(\alpha, e) = \alpha^{-2} \frac{(1+e)^2}{2e} \ln \frac{1+e}{1-e} \quad (\text{singular isothermal sphere}). \quad (\text{B2d})$$

Now we integrate the orbit using the quadratures:

$$\theta = \int_{r_p}^r \frac{dr}{r^2 \left(\frac{2\varepsilon - 2\phi(r)}{j^2} - \frac{1}{r^2} \right)^{1/2}} \quad (\text{B3a})$$

$$t = \int_{r_p}^r \frac{dr}{j \left(\frac{2\varepsilon - 2\phi(r)}{j^2} - \frac{1}{r^2} \right)^{1/2}}, \quad (\text{B3b})$$

where r is the dimensionless radius, $r \equiv R/a$ or $r \equiv R/R_{max}$, and ε is the dimensionless energy of the orbit. To avoid singularities at both perigalacticon and apogalacticon, we divide the integrals into two parts at some intermediate radius $r_{div} \equiv (1+e)r_p$. Then, we change the variables of integration separately for the two parts to remove the singularity. For $r_p \leq r \leq r_{div}$, the new variable is $u_1 \equiv \sqrt{\alpha - \frac{1}{r}}$; for $r_{div} \leq r \leq r_a$, the new variable is $u_2 \equiv \sqrt{\frac{1}{r} - \alpha \frac{1-e}{1+e}}$. Both parts of the integral are regular in u_1 or u_2 and can be calculated numerically with high accuracy.

Note that in the harmonic oscillator potential the orbits allow simple analytic representation. In Cartesian coordinates,

$$x = r_p \cos t, \quad y = r_a \sin t, \quad (\text{B4})$$

where

$$t = \arctan \left(\frac{1-e}{1+e} \tan \theta \right). \quad (\text{B5})$$

REFERENCES

Aguilar, L., Hut, P., & Ostriker, J. P. 1988, *ApJ*, 335, 720

Aguilar, L. A., & White, S. D. M. 1985, *ApJ*, 295, 374

Bahcall, J. N., Schmidt, M., & Soneira, R. M. 1983, *ApJ*, 265, 730

Binney, J., & Tremaine, S. 1987, *Galactic Dynamics* (Princeton: Princeton Univ. Press)

Gnedin, O. Y., & Ostriker, J. P. 1997a, *ApJ*, 474, 223

Gnedin, O. Y., & Ostriker, J. P. 1997b, *ApJ*, submitted

Hernquist, L. 1990, *ApJ*, 356, 359

Hernquist, L., & Ostriker, J. P. 1992, *ApJ*, 386, 375

Johnston, K.V., Hernquist, L., & Weinberg, M.D. 1997, *ApJ*, submitted

Knobloch, E. 1976, *ApJ*, 209, 411

Ostriker, J. P., & Caldwell, J. A. 1983, in *Kinematics, Dynamics and Structure of the Milky Way*, ed. W. L. H. Shuter (Dordrecht: Reidel), 249

Richstone, D. 1975, *ApJ*, 200, 535

Spitzer, L. Jr. 1958, *ApJ*, 127, 17

Spitzer, L. Jr. 1987, *Dynamical Evolution of Globular Clusters* (Princeton: Princeton Univ. Press)

Weinberg, M. D. 1994, *AJ*, 108, 1403

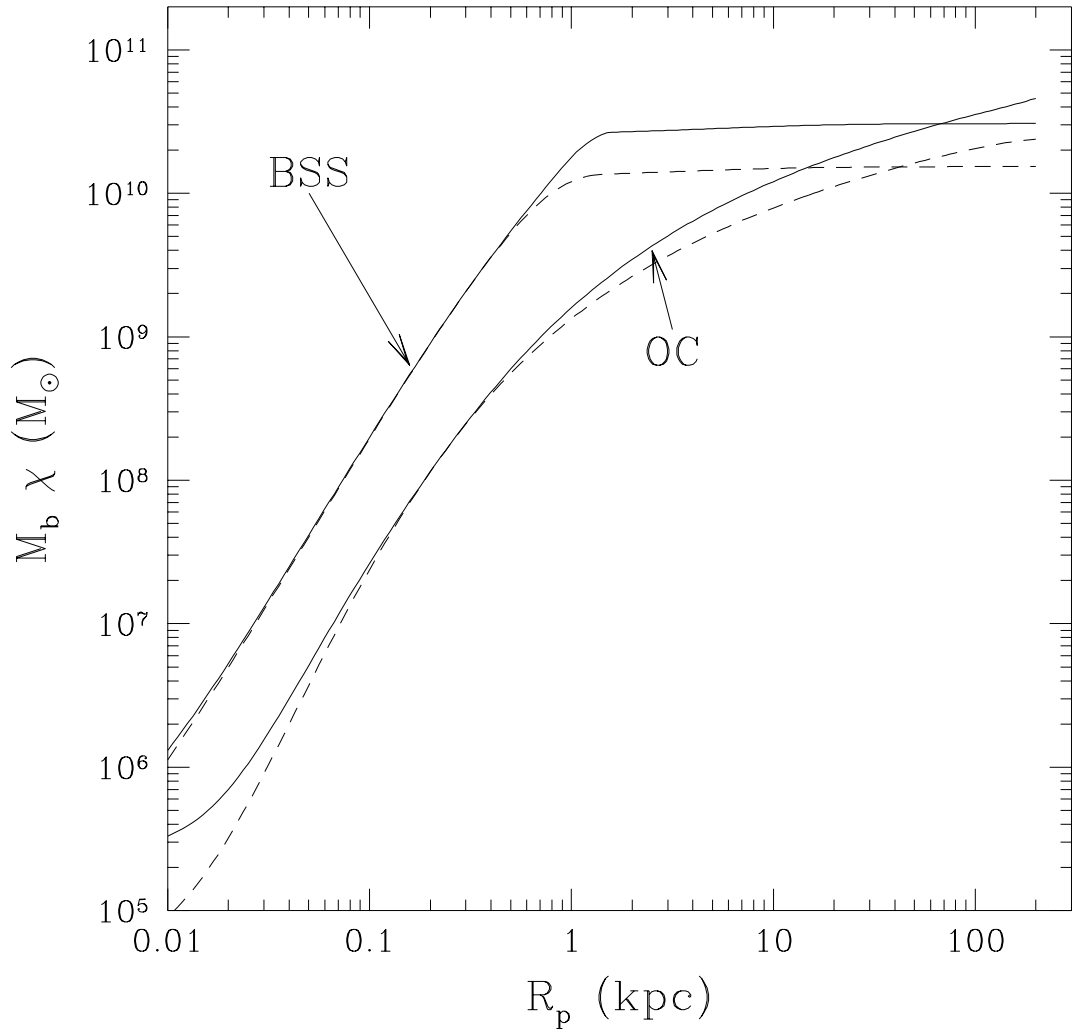


Fig. 1.— Correction factors $\chi_{st}(R_p)$ for the extended mass distribution of the Galactic bulge for two models of the Galaxy: Ostriker & Caldwell (1983) and Bahcall, Schmidt, & Soneira (1983). Our function [eq. (14)] is shown by the solid curve, and that from Aguilar & White (1985) is given by the dashes. For convenience, both functions are normalized to the total mass of the bulge, M_b , in each Galactic model, respectively.

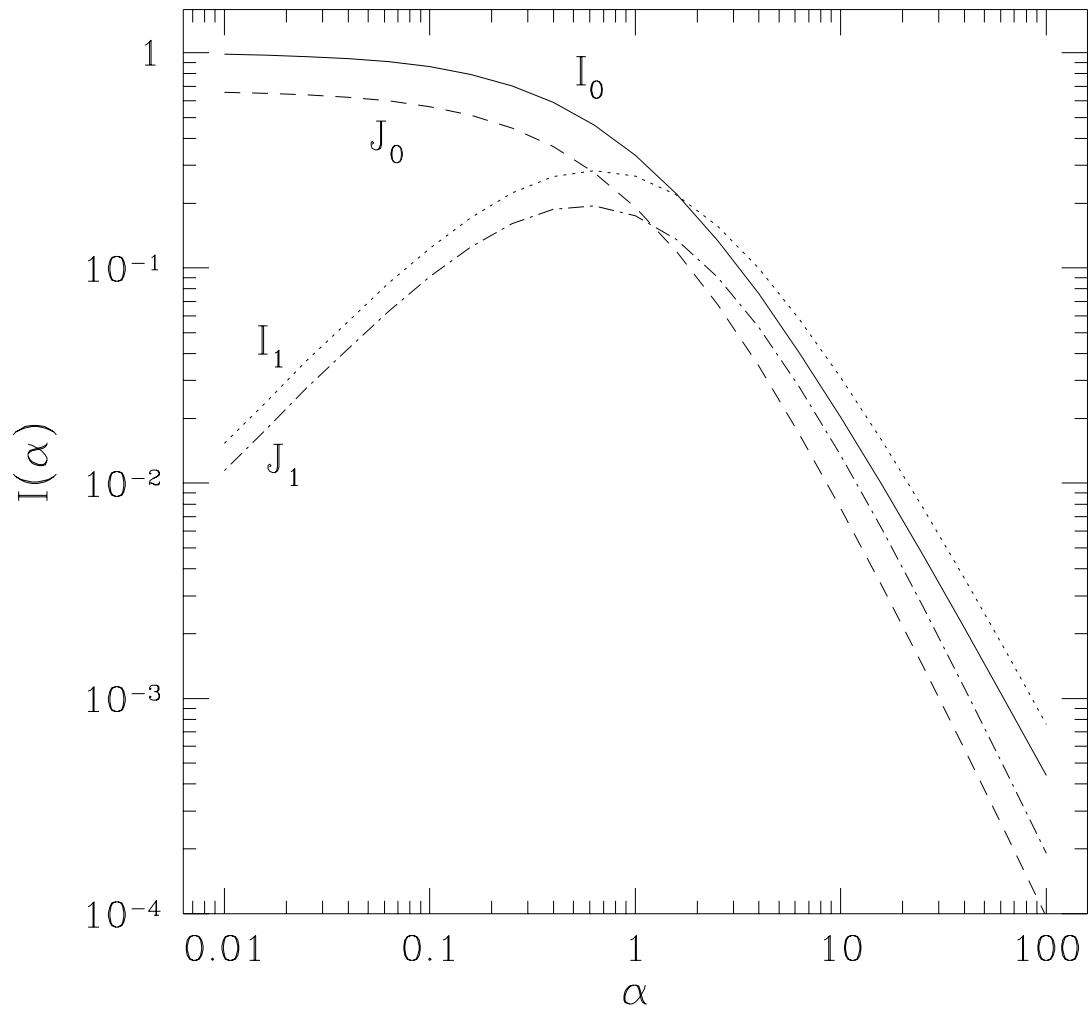


Fig. 2.— Integrals I_0 , J_0 , I_1 , and J_1 (eq. [A9]) for the Hernquist model.

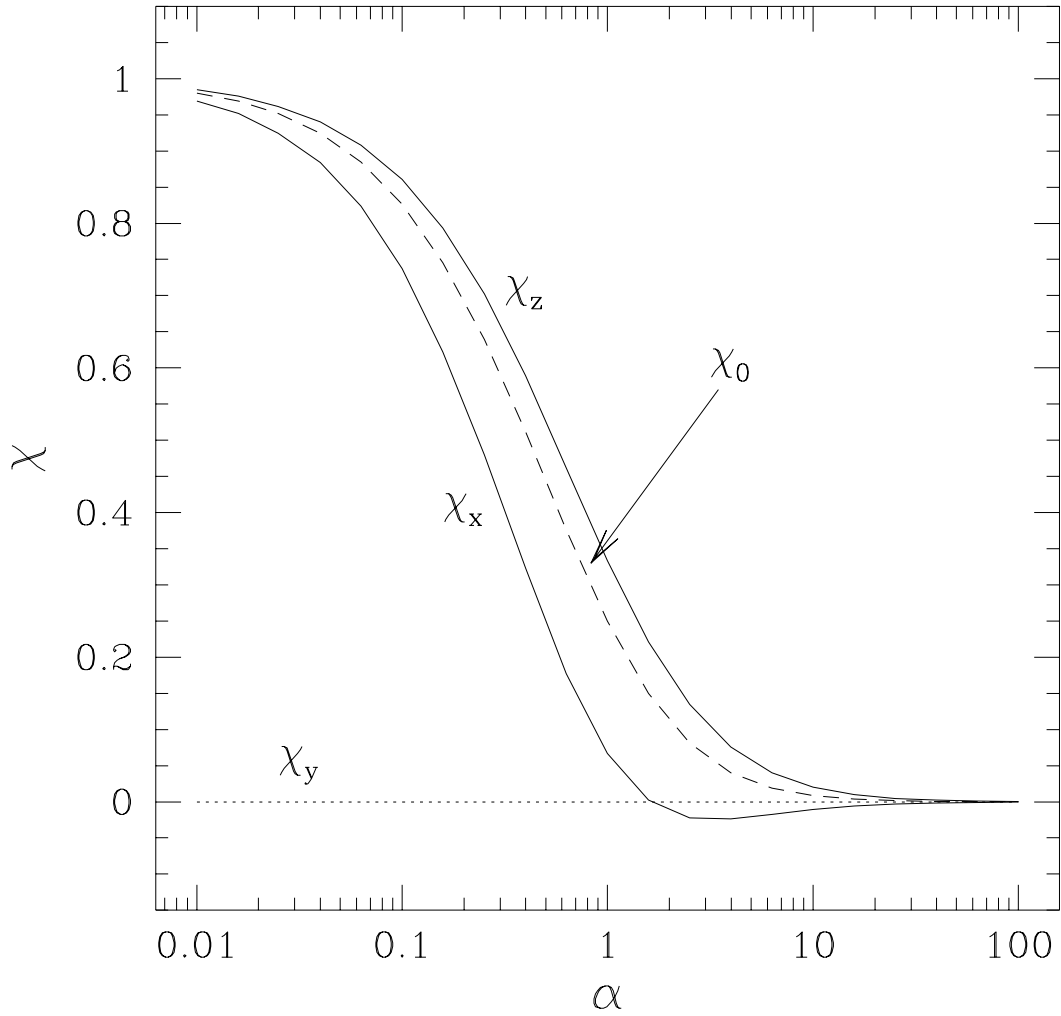


Fig. 3.— Corrections to the velocity change for a Hernquist model (cf eq. [20]). The components χ_x and χ_z are relative to their values in the point-mass approximation, while χ_y is always close to zero, as it would be in a point-mass potential. Plotted for comparison is the approximation when the galactic mass inside the satellite perigalacticon is taken to be a point-mass ($\chi_0 = \mu(R_p)$).

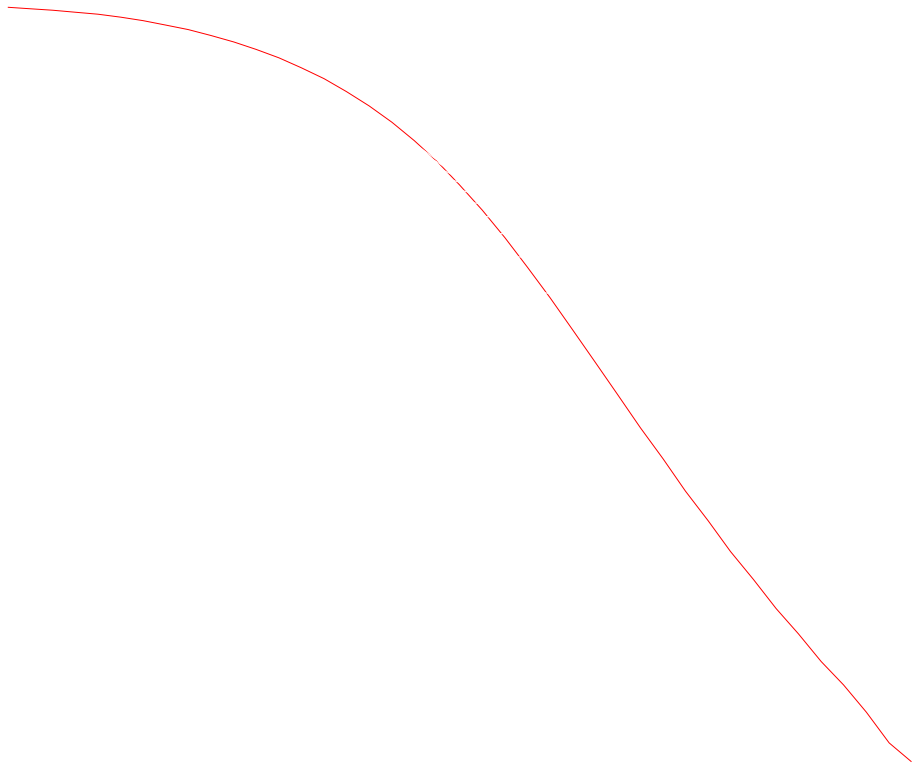


Fig. 4.— The ratio of the correction factors χ_{ecc}/χ_{st} for the extended mass distribution of the host galaxy for eccentric and straight orbits of the satellite. The lines correspond to the orbits with eccentricities running from 0 to 1 with a step of 0.1, in the Hernquist model for the galaxy. $\alpha \equiv a/R_p$, where a is the scale length of the Hernquist model and R_p is the perigalacticon of the orbit. In the calculation of each curve we assumed the same angular momentum of the straight orbit as for the corresponding eccentric orbit. Accordingly, the denominator χ_{st} may vary for each line. Adiabatic corrections are not included. Had they been, the correction factors for $e \rightarrow 0$ would have been reduced dramatically.

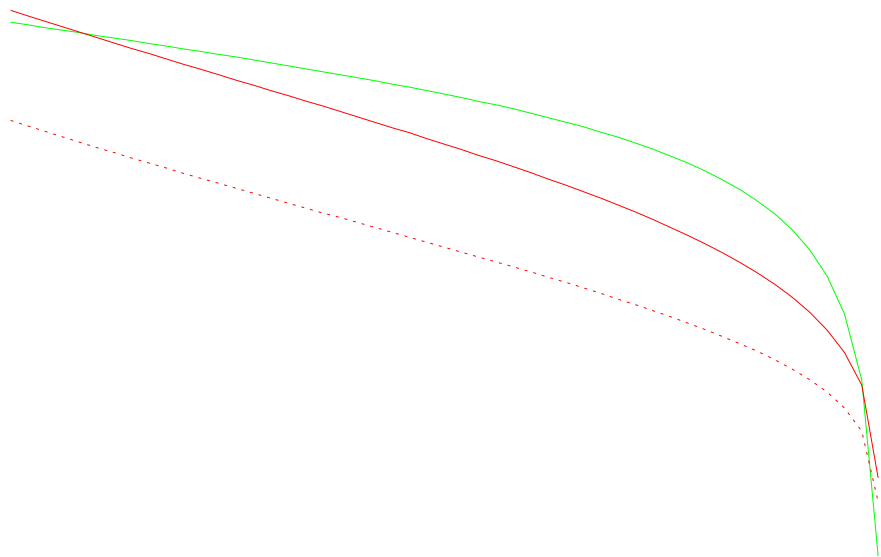


Fig. 5.— The correction factor χ_{ecc} for the power-law models (eq. [35]) versus eccentricity of the orbit. For the isothermal sphere ($n = 2$), we also show the straight-path approximation, χ_{st} (dots).

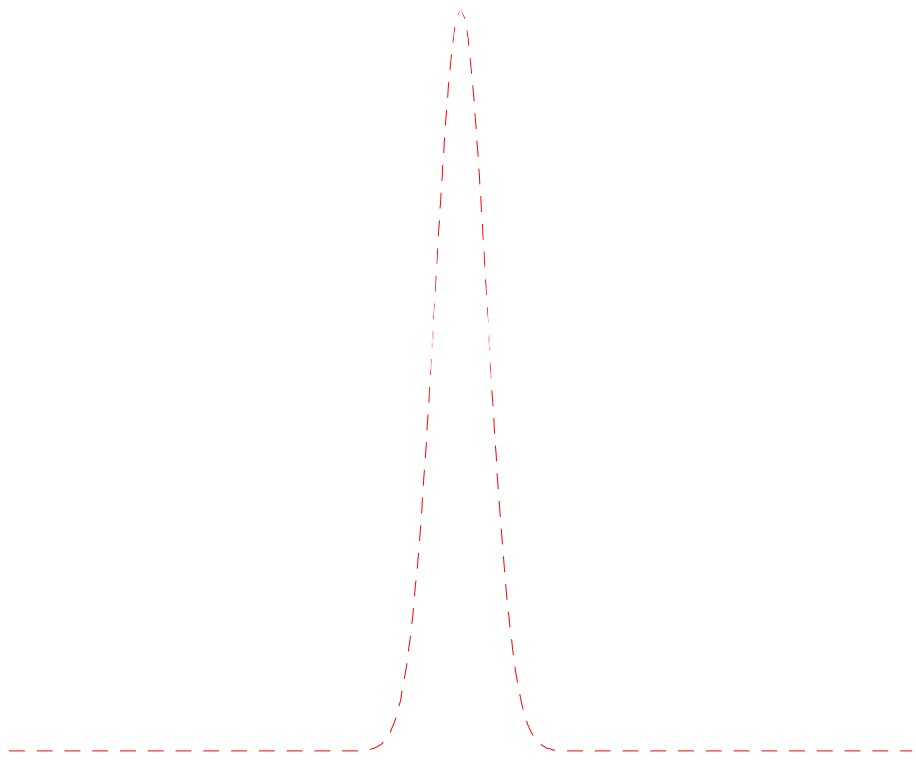


Fig. 6.— The time variation of the vertical component of the tidal force exerted on globular cluster NGC 6712 by the Galactic bulge. Solid line is the actual force, whereas the dashes are for the Gaussian fit with the effective width $\tau = 5.3 t_{dyn}$. The force is in the units of the N-body code.

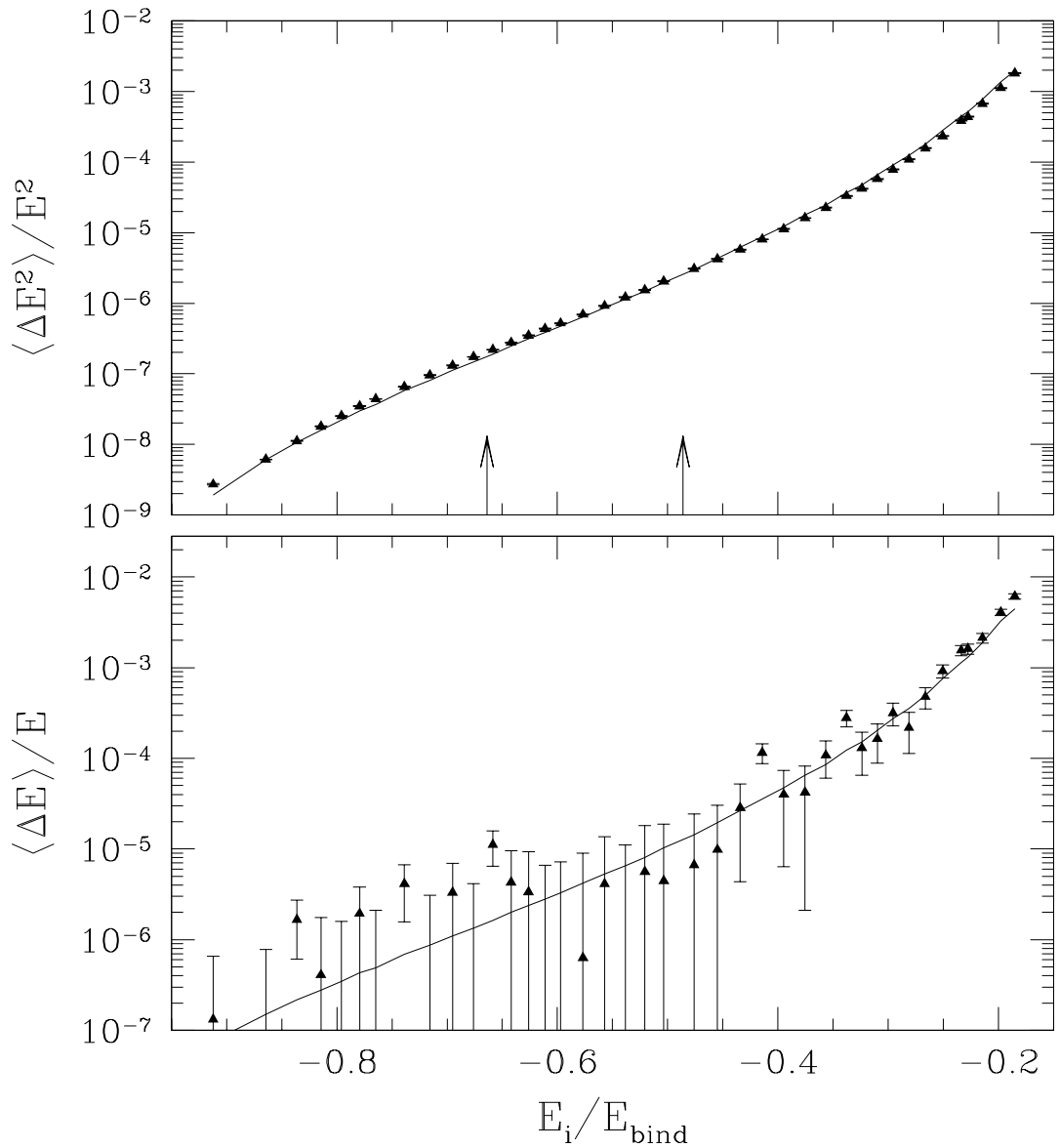


Fig. 7.— The first and second order energy changes for globular cluster NGC 6712. Both changes are plotted versus the initial energy of the stars, E_i , and are normalized to the corresponding power of E_i . E_{bind} is the initial binding energy of the system. The arrows show the core radius and the half-mass radius of the cluster. The lines are the analytic fits (eq. [31]). Error-bars indicate the standard deviations for each bin.

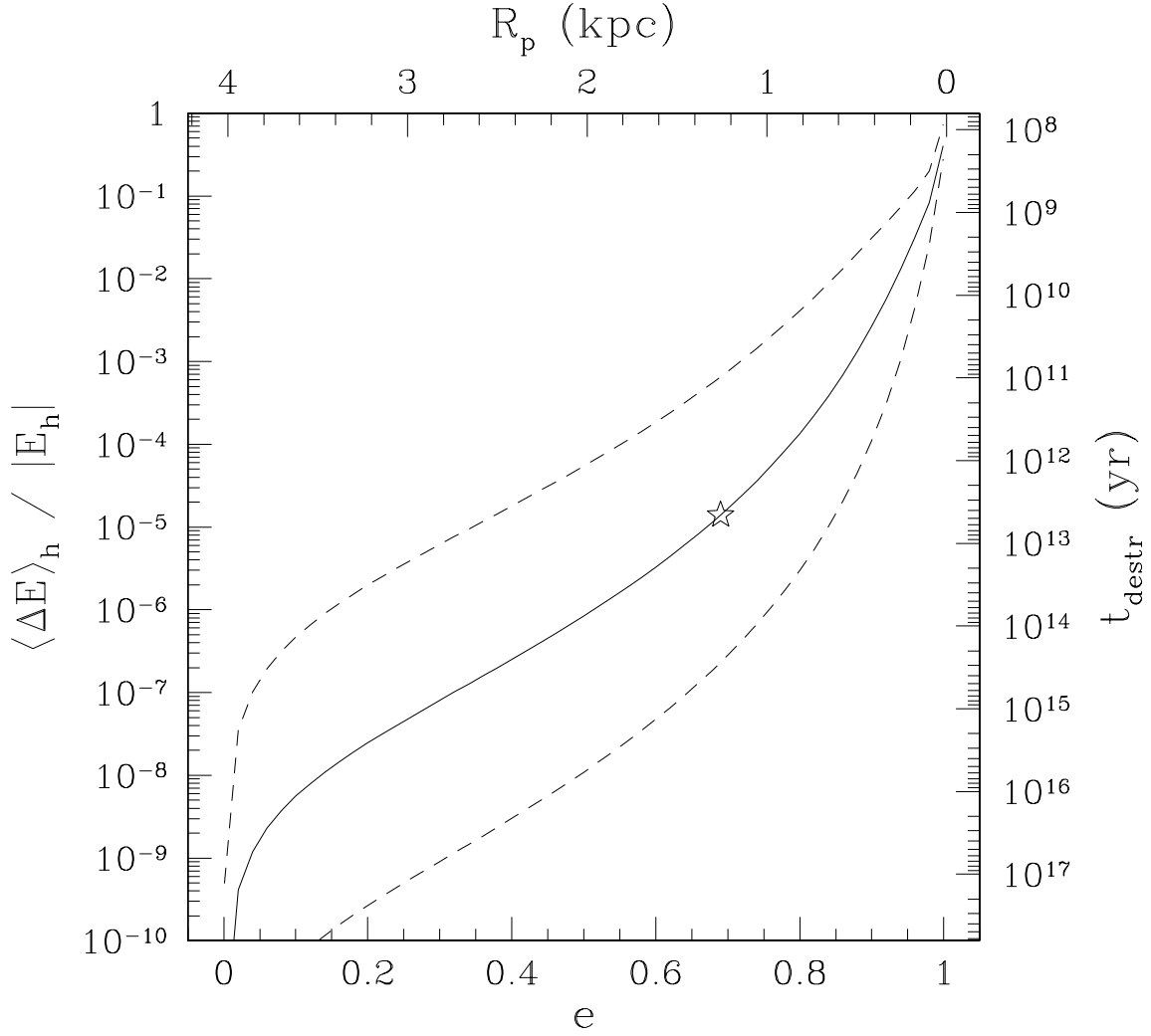


Fig. 8.— The energy change of stars at the half-mass radius of NGC 6712 relative to the initial half-mass energy as a function of eccentricity of the orbit, e , or the corresponding perigalactic distance, R_p . The orbital energy is fixed at the observed value for the cluster (solid line) or at one-half and twice that value (dashed lines below and above the solid line, respectively). The star marks the eccentricity of NGC 6712 in our kinematic model (see §4.1). For illustration, we also show on the right-hand-side axis the approximate destruction time of the cluster due only to tidal shocks. The destruction time is defined as $t_{\text{destr}} \equiv P_{\text{orb}}(E_h/\Delta E_h)$, where P_{orb} is the cluster orbital period, which varies with the eccentricity. In contrast to Figure 4, which did not allow for adiabatic corrections, we see that tidal shocking vanishes as $e \rightarrow 0$.